

# Two close binaries across the hydrogen-burning limit in the Praesepe open cluster

N. Lodieu<sup>1,2\*</sup>, C. del Burgo<sup>3,1</sup>, E. Manjavacas<sup>4,5</sup>, M. R. Zapatero Osorio<sup>6</sup>, C. Alvarez<sup>4</sup>, V. J. S. Béjar<sup>1,2</sup>, S. Boudreault<sup>7</sup>, J. Lyke<sup>4</sup>, R. Rebolo<sup>1,2,8</sup>, P. Chinchilla<sup>1,2</sup>

<sup>1</sup>*Instituto de Astrofísica de Canarias Calle Vía Láctea S/N 38205 La Laguna, Tenerife, Spain*

<sup>2</sup>*Departamento de Astrofísica, Universidad de La Laguna (ULL), E-38206 La Laguna, Tenerife, Spain*

<sup>3</sup>*Instituto Nacional de Astrofísica, Óptica y Electrónica, Luis Enrique Erro 1, Sta. Ma. Tonantzintla, Puebla, Mexico*

<sup>4</sup>*W. M. Keck Observatory, 65-1120 Mamalahoa Hwy, Kamuela, HI, 96743, USA*

<sup>5</sup>*Department of Astronomy/Steward Observatory, The University of Arizona, 933 N. Cherry Avenue, Tucson, AZ 85721, USA*

<sup>6</sup>*Centro de Astrobiología (CSIC/INTA), 28850 Torrejón de Ardoz, Madrid, Spain*

<sup>7</sup>*Max-Planck-Institut für Sonnensystemforschung, Justus-von-Liebig-Weg 3, 37077, Göttingen, Germany*

<sup>8</sup>*Consejo Superior de Investigaciones Científicas, CSIC, Spain*

Accepted XXX. Received YYY; 18 March 2022

## ABSTRACT

We present Keck I/OSIRIS and Keck II/NIRC2 adaptive optics imaging of two member candidates of the Praesepe stellar cluster ( $d = 186.18 \pm 0.11$  pc; 590–790 Myr), UGCS J08451066+2148171 (L1.5 $\pm$ 0.5) and UGCS J08301935+2003293 (no spectroscopic classification). We resolved UGCS J08451066+2148171 into a binary system in the near-infrared, with a  $K$ -band wavelength flux ratio of  $0.89 \pm 0.04$ , a projected separation of  $60.3 \pm 1.3$  mas ( $11.2 \pm 0.7$  au;  $1\sigma$ ). We also resolved UGCS J08301935+2003293 into a binary system with a flux ratio of  $0.46 \pm 0.03$  and a separation of  $62.5 \pm 0.9$  mas. Assuming zero eccentricity, we estimate minimum orbital periods of  $\sim 100$  years for both systems. According to theoretical evolutionary models, we derive masses in the range of  $0.074$ – $0.078 M_{\odot}$  and  $0.072$ – $0.076 M_{\odot}$  for the primary and secondary of UGCS J08451066+2148171 for an age of  $700 \pm 100$  Myr. In the case of UGCS J08301935+2003293, the primary is a low-mass star at the stellar/substellar boundary ( $0.070$ – $0.078 M_{\odot}$ ) while the companion candidate might be a brown dwarf ( $0.051$ – $0.065 M_{\odot}$ ). These are the first two binaries composed of L dwarfs in Praesepe. They are benchmark systems to derive the location of the substellar limit at the age and metallicity of Praesepe, determine the age of the cluster based on the lithium depletion boundary test, derive dynamical masses, and improve low-mass stellar and substellar evolutionary models at a well-known age and metallicity.

**Key words:** (stars:) binaries: general – stars: late-type – open clusters: Praesepe

## 1 INTRODUCTION

The fate of a star is primarily set by its mass. Dynamical masses of single and multiple stellar and substellar systems serve as valuable input to constrain theoretical evolutionary models and to compare with predictions of physical parameters by star and brown dwarf formation models (Zapatero Osorio et al. 2004; del Burgo & Allende Prieto 2018). Brown dwarfs cool down as they age, meaning that their masses are challenging to determine without precise values for their age.

Hence, studying multiple systems at the hydrogen-burning limit at different ages and metallicities is of prime interest to derive dynamical masses, locate the stellar/substellar boundary, and calibrate evolutionary models.

The number of low-mass stars with wide ultracool and substellar companions has significantly increased over the past decades with independent dedicated surveys in star-forming regions (Ahmic et al. 2007; Kraus et al. 2006; Todorov et al. 2010), OB associations (Kraus et al. 2005; Bouy et al. 2006a; Biller et al. 2011), young moving groups (Naud et al. 2017), intermediate-age clusters such as the Pleiades (Martín et al. 2000, 2003; Bouy et al. 2006b),

\* E-mail: nlodieu@iac.es (NL)

and older clusters like the Hyades (Duchêne et al. 2013), and in the field (e.g. Burgasser et al. 2007; Dupuy & Liu 2017). Additional discoveries have been reported as part of studies involving smaller sample sizes in diverse regions such as Orion (Stassun et al. 2006), Taurus (Todorov et al. 2010; Konopacky et al. 2007), LkH $\alpha$ 233 (Allers et al. 2009), Chamaeleon (Joergens 2006; Joergens & Müller 2007; Joergens 2008), Upper Scorpius (Béjar et al. 2008; Chinchilla et al. 2020), R Corona Australis (Bouy et al. 2004), TW Hydra (Chauvin et al. 2005; Mohanty et al. 2007), AB Doradus (Desrochers et al. 2018), and Tucana-Horologium (Artigau et al. 2015). These studies, among others, seem to point towards a gradual decline of multiplicity with mass and limited differences as a function of age, although not all surveys map the same mass and separation intervals. Nonetheless, binary systems are of prime importance to scale masses as a function of age and improve stellar evolutionary models (e.g. Baraffe et al. 2015).

The Praesepe cluster (a.k.a. the Beehive cluster, M44) is relatively young and one of the nearest clusters to the Sun. It is located at a distance of  $186.18 \pm 0.11$  pc (Gaia Collaboration et al. 2018b,a; Lindegren et al. 2018) with a tidal radius of 10.7 pc (Lodieu et al. 2019). We adopt these values throughout the analysis presented in this paper. The range in age, 590–790 Myr, is debated in the literature (Mermilliod 1981; Fossati et al. 2008; Delorme et al. 2011; Brandt & Huang 2015a; Gossage et al. 2018), but comparable to the Hyades (Maeder & Mermilliod 1981; Brandt & Huang 2015b; Martín et al. 2018; Lodieu et al. 2018a). Members of Praesepe share a significant proper motion ( $\mu_{\alpha} \cos(\delta)$ ,  $\mu_{\delta}$ ) allowing an astrometric selection which coupled with photometry led to a pre-*Gaia* census of more than 1100 member candidates from high-mass stars down to the substellar regime (Hambly et al. 1995; Adams et al. 2002; Kraus & Hillenbrand 2007; Pinfield et al. 1997; Chappelle et al. 2005; González-García et al. 2006; Boudreault et al. 2010; Baker et al. 2010; Wang et al. 2011; Boudreault et al. 2012; Khalaj & Baumgardt 2013; Wang et al. 2014).

Boudreault et al. (2012) presented a pre-*Gaia* updated census of photometric and astrometric cluster member candidates down to the hydrogen-burning limit in 36 square degrees of Praesepe surveyed by the UKIRT Infrared Deep Sky Survey Galactic Clusters Survey (Lawrence et al. 2007). In a sample of over 1100 member candidates, Boudreault & Lodieu (2013) confirmed spectroscopically the first L-type member, UGCS J084510.66+214817.1 (hereafter UGCS0845), classified as an  $L0.3 \pm 0.4$  dwarf with an effective temperature of  $\sim 2300$  K and a mass of  $71.1 \pm 23.0 M_{\text{Jup}}$ . Moreover, they proposed UGCS0845 as a photometric binary candidate because of its location above the cluster sequence in several colour-magnitude diagrams (Fig. 1). Other member candidates lie in the potential binary sequence of Praesepe.

In this paper, we present high spatial resolution imaging of UGCS0845 and UGCS J08301935+2003293 (hereafter UGCS0830). They have been confirmed as members of the Praesepe cluster based on their astrometry and photometry, and the latter also spectroscopically. In Section 2 we present optical and near-infrared spectroscopy of UGCS0845. In section 3 we describe the adaptive optics campaign confirming both sources as visual binaries. In Section 4 we infer their physical parameters, including separations, bolometric lu-

minosities, and masses. We put our results in context and discuss their impact in Section 5.

## 2 OPTICAL AND NEAR-INFRARED SPECTROSCOPY

### 2.1 Near-infrared spectroscopy

We observed UGCS0845 with the X-shooter spectrograph (D’Odorico et al. 2006; Vernet et al. 2011) on the European Southern Observatory (ESO) Very Large Telescope arrays (VLT) on the night of 01 January 2017 between 6h and 7h UT as part of programme number 098.C-0277(A) (P.I. Manjavacas). The sky was clear with a seeing of 0.6–0.9 arcsec and the moon illuminated at 65%.

X-shooter is composed of three arms covering the ultraviolet (UVB; 300–550 nm), visible (VIS; 550–1000 nm), and near-infrared (NIR; 1000–2500 nm). We used slits of 1.3 arcsec in the UVB and 1.2 arcsec in the VIS and NIR, yielding resolving powers of  $\sim 2030$  in the UVB,  $\sim 3360$  in the VIS, and  $\sim 3900$  in the NIR. We collected 10 individual frames of 300 s with an AB pattern and an offset of 6 arcsec to optimise sky subtraction in the NIR. We observed at parallactic angle to mitigate the effect of differential chromatic refraction. Due to the low signal to noise in the UVB and VIS arms, we only analyse the NIR spectrum. We observed the telluric standard star HIP 026545 at a similar airmass just after our target. Bias, flats, and arc lamps were collected as part of the ESO calibration plan.

We reduced the spectra with the X-Shooter pipeline version 1.3.7 (Goldoni et al. 2006; Modigliani et al. 2010), which deals with the main instrumental effects to produce a 2D combined image for each arm. We optimally extracted the NIR spectrum with the task `apa11` in IRAF (Tody 1986, 1993)<sup>1</sup>. We used the spectrum of the telluric standard to obtain the instrument response function and correct for telluric features. Then, we derived a response function by dividing the non-flux calibrated spectrum of the telluric standard (cleaned of cosmic rays and strong telluric lines) by a blackbody synthetic spectrum with the same temperature as the B-type telluric (Theodossiou & Danezis 1991). Finally, we divided the spectrum of UGCS0845 by this response function to correct for the instrumental response and telluric lines. We display the X-shooter NIR spectrum in the right-hand side panel of Fig. 2.

### 2.2 Optical spectroscopy

We obtained a low-resolution optical spectrum of UGCS0845 on 16 January 2013 with the OSIRIS instrument (Optical System for Imaging and low Resolution Integrated Spectroscopy; Cepa et al. 2000) mounted on the 10.4 m Gran Telescopio Canarias (GTC) in the Roque de Los Muchachos Observatory in La Palma (Canary Islands) under program GTC66-12B (PI Boudreault). The observing conditions were

<sup>1</sup> IRAF is distributed by the National Optical Astronomy Observatory, which is operated by the Association of Universities for Research in Astronomy (AURA) under a cooperative agreement with the National Science Foundation

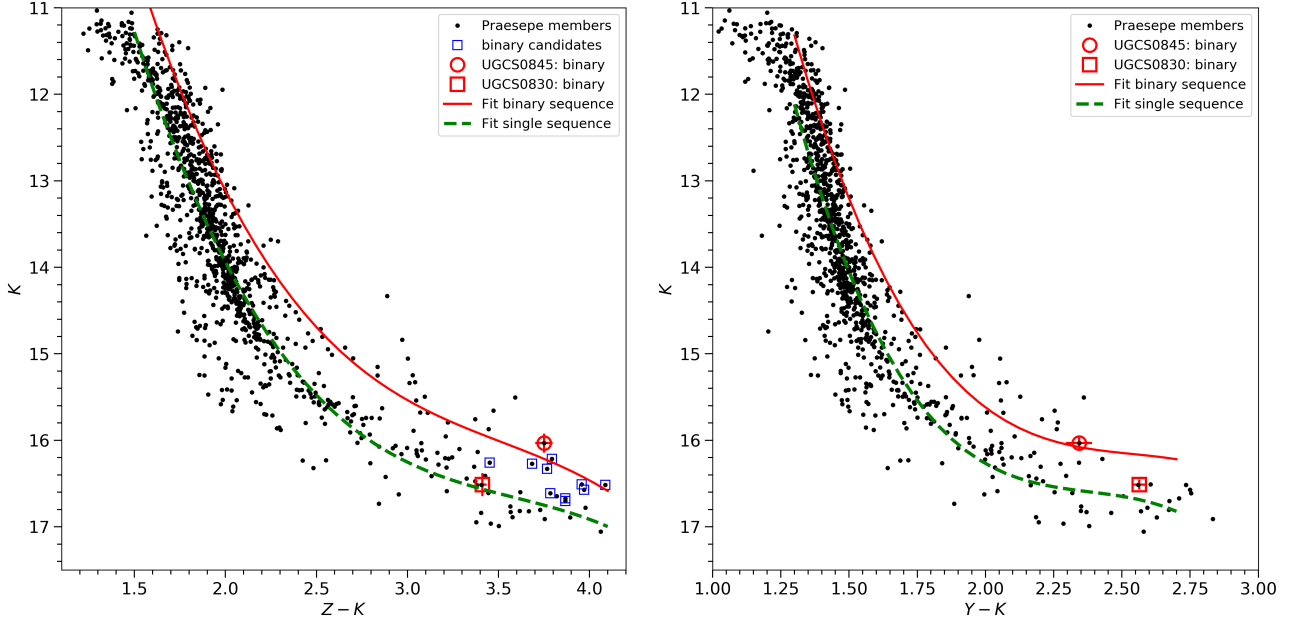


**Figure 1.** *Left:*  $(Z - K, K)$  colour-magnitude diagram showing the position of UGCS0845 (red circle) and UGCS0830 (red square) close to the binary sequence (red line) of the cluster, which contains over 1100 members (black dots; Boudreault et al. 2012). *Right:*  $(Y - K, K)$  colour-magnitude diagram. The green and red lines represent fits to the single and equal-mass binary sequences of the cluster.

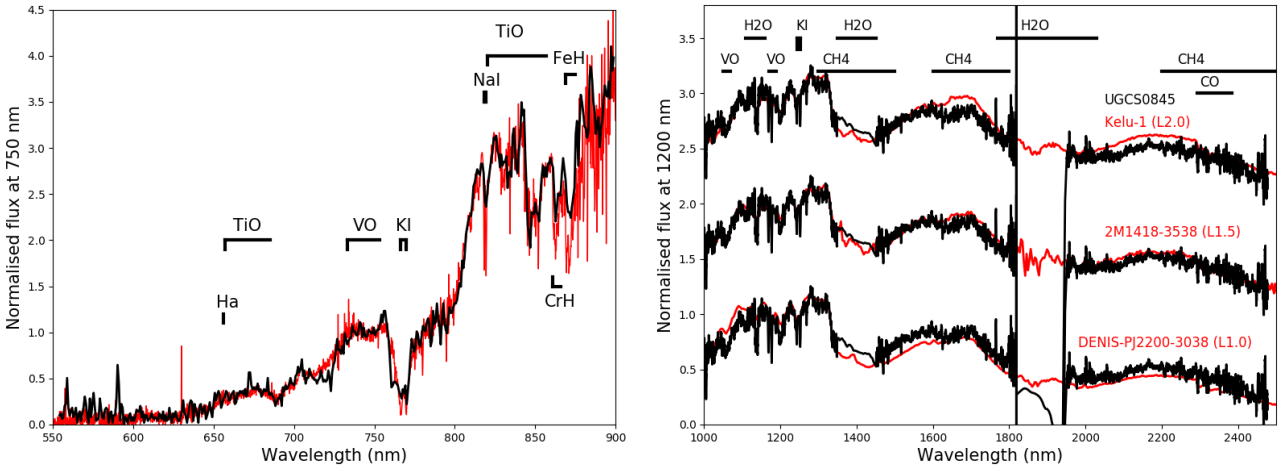


**Figure 2.** *Left:* GTC/OSIRIS low-resolution optical spectrum of UGCS0845 (black) compared with the best fit (L1.0; red) from the Sloan database of L dwarfs (Schmidt et al. 2010). The GTC spectrum is not corrected for telluric absorption while the Sloan one is. *Right:* VLT/X-shooter near-infrared spectrum of UGCS0845 (black) compared to three L dwarf very low resolution spectra (Ruiz et al. 1997; Kendall et al. 2004; Burgasser & McElwain 2006; Burgasser 2007; Kirkpatrick et al. 2010) downloaded from the SpeX archive (red). Main spectral features are highlighted.

spectroscopic (thin cirrus) with a seeing better than 1.2 arcsec and no moon. We used the  $2 \times 2$  binning mode of OSIRIS with the R300R grism and a 1.2 arcsec slit width, yielding a resolving power of  $\sim 350$  at 685 nm. This configuration shows contamination from the second-order light redwards of 850 nm, although it becomes stronger at  $>900$  nm. We did not correct for this contamination, hence limiting our wavelength range to 550–900 nm.

We collected six spectra with an integration time of 700 s each, and applied an offset of 10 arcsec along the slit to ease removal of artifacts and cosmic rays. We reduced the

spectrum in a standard manner, removing bias and flat-field from the 2D images, combining the six spectra, and optimally extracting the combined spectrum with `apall` as in the case of X-shooter. We calibrated the spectrum in wavelength with a combination of HgAr, Ne, and Xe lamps with a rms better than  $0.5 \text{ \AA}$ . We applied the response function to UGCS0845 using the spectro-photometric standard star Ross 640 (Oke 1990) observed with the same set-up on the same night as our target. The final spectrum, uncorrected for telluric contribution, is presented in the left-hand panel

of Fig. 2 along with the best fit using an Sloan L dwarf template (Schmidt et al. 2010).

### 3 LASER GUIDE STAR ADAPTIVE OPTICS IMAGING

#### 3.1 Keck/OSIRIS observations

We observed UGCS0845 on 20 November 2018 using the OH-Suppressing Infra-Red Imaging Spectrograph (OSIRIS) instrument (Larkin et al. 2006) on the Keck I telescope. We obtained a second epoch on 24 January 2019. OSIRIS is a near-IR imager and integral field spectrograph coupled to the Keck Adaptive Optics (AO) system (Wizinowich et al. 2006; van Dam et al. 2006). Observations were performed in Laser-Guide-Star (LGS) mode with the recently-upgraded imaging arm of OSIRIS (Arriaga et al. 2018). The OSIRIS imager has a pixel scale of  $\sim 0.010$  arcsec and a field of view of  $20'' \times 20''$ . We used the  $K_p$  filter ( $\lambda_c = 2.144\mu\text{m}$ ,  $\Delta\lambda = 0.307\mu\text{m}$ ) on a five-point dither pattern with an integration time of 57.5 seconds per position. Additionally, we observed the astrometric binary ADS 3279 AB with the  $K_{cont}$  filter ( $\lambda_c = 2.270\mu\text{m}$ ,  $\Delta\lambda = 0.02\mu\text{m}$ ) on 22 November 2018 to determine the plate scale of the detector with good precision. The integration time on ADS 2279 AB was 1.475 seconds. The sky was clear and the seeing below 0.8 arcsec on both nights.

Additionally, we observed UGCS0845 and UGCS0830 on 22 March 2019 with Keck I/OSIRIS. The sky was clear and the seeing sub-arcsec. For each target, we collected five exposures of 15 seconds each with the  $K_p$  filter using a small dither pattern.

We reduced the data with IRAF routines (Tody 1986, 1993) following standard procedures in the near-infrared. We obtained uniformly illuminated images by dome lights and combined them to create a flat-field image. We flat-fielded the raw frames of the targets and later combined them with a median filter to remove the stars and create a sky background image. We sky-subtracted these images, aligned them, and combined them to produce the final deep image.

The offsets in the dithering pattern of the images collected for UGCS0830 turned out to be too small for a proper sky subtraction. Hence, we directly used the original images, without additional treatment.

To measure the plate scale, we used three independent images of the binary ADS 3297 AB (HD 28867) obtained on 2018 November 22 and the astrometry given by *Gaia* DR2, which is consistent with that of Scardia et al. (2007), although with significantly higher precision. According to *Gaia*, the projected separation of the two stars is  $3.06823 \pm 0.00010$  arcsec. We calculated a pixel size of the Keck/OSIRIS detector of  $9.9407 \pm 0.0071$  mas, assuming squared pixels. The uncertainty accounts for the dispersion of the measurements.

#### 3.2 Keck/NIRC2 observations

We observed UGCS0845 and UGCS0830 with the NIRC2 instrument on the Keck II telescope in LGS-AO mode on 11 March 2020 between UT 06h40m and 07h10m. The sky

was clear and the seeing was sub-arcsec. We employed the  $K_s$  filter and the NIRC2 narrow field camera with a pixel scale of  $9.971 \pm 0.004$  mas (Service et al. 2016) and a field of view of  $10 \times 10$  arcsec<sup>2</sup>. Observations were taken following a 3-point dither pattern with offsets of five arcsec, a jitter of a few pixels, and an on-source integration time of 60s per dither position. This pattern was repeated three times, thus yielding a total exposure time of nine min per target. We avoided the lower left quadrant of the NIRC2  $1024 \times 1024$  Aladdin-3 InSb detector, since it is known to be slightly noisier than the other three quadrants. We note that the images of UGCS0845 suffer from elongation due to wind shake in the direction of the telescope elevation at the time of the observations, making this dataset not usable.

We reduced the data in a standard manner under the IRAF environment. We median-combined the nine raw frames per target to create a sky image. We subtracted this sky frame from each individual raw image before aligning and stacking all data to produce the final, deep image.

We also observed the astrometric binary ADS 7878 AB on 11 March 2020. We used the position angle of ADS 7878 AB from Scardia et al. (2007),  $161.9 \pm 0.3$  deg, to determine the orientation of the NIRC2 FOV with respect to the celestial equatorial system.

## 4 PHYSICAL PARAMETERS

### 4.1 Method: PSF decomposition

The separation of the two components of the systems presented in this work is below the full width half maximum (FWHM) of single objects observed with the same correction. We apply a method based on point-spread function (PSF) reconstruction to estimate the most likely flux ratio, FWHM, the angle between the line defined by the centroids of the binary components and a reference axis (vertical), and the angular separation of the components. We assumed that the PSF is the same at the positions of the binary components (for the two cases discussed here) given their small angular separation on the OSIRIS detector (Fig. 3).

The method outlined in Fig. 3 is able to separate the two components of the binaries. In both cases the primary (hereinafter P1) is below the secondary (P2). The image of each component was reconstructed after joining the flux signal above the top line with that below the bottom line, conveniently scaled and shifted. For example, for the primary, we leave untouched the signal below the bottom line and then shifted and scaled the signal above the top line to complete its shape. We applied a bi-linear interpolation method to shift the data (left in Fig. 3).

We apply the aforementioned approach taking into account four free parameters: the flux ratio between the secondary and the primary, the multiplicative factor  $\gamma$  with values between 0 and 1, the angle of the straight lines (parallel between them) with respect to the x axis, and the zero points in the y axis for the upper and lower straight lines.

After reconstructing the image of a given component (for every trial), we subtracted it from the original image (O). In this way, we derive the image of the companion in a different way. We took the average of the two versions for every component. The method attempts to reduce the



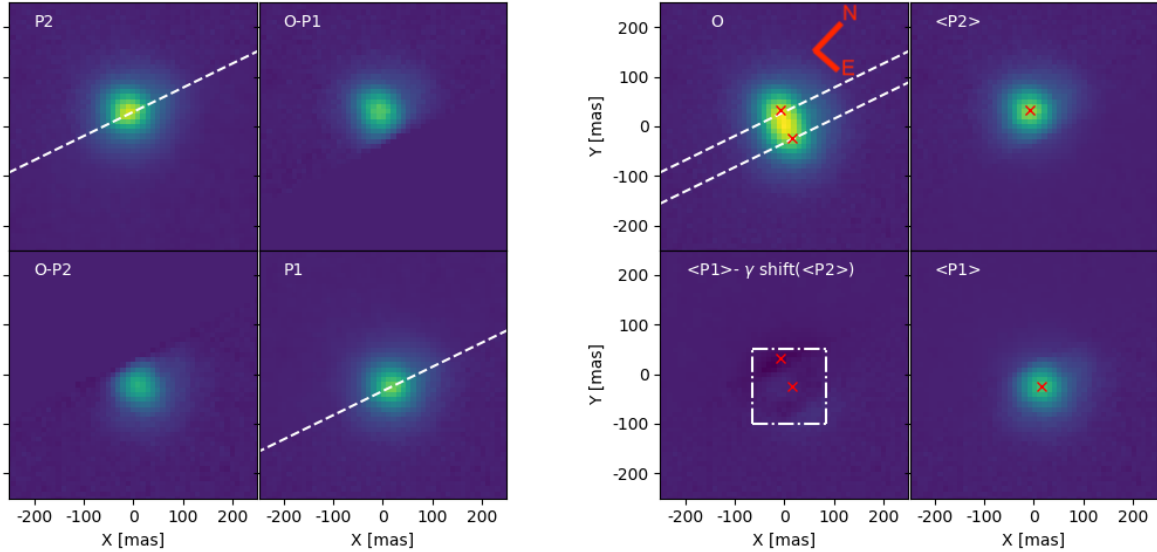


**Figure 3.** *Left panel:* Illustration of the PSF decomposition method used for both instruments. The top-left plot shows the OSIRIS image of the secondary P2, obtained from taking the signal over the dashed line and under the dashed line in the bottom-right plot, but with the signal shifted to the position and multiplied by the flux ratio. The bottom-right plot illustrates the same but for the primary. The top-right (bottom-left) plot displays the result of subtracting image P1 (P2) to image O, providing a second version for the secondary (primary). *Right panel:* Reconstruction of the UGCS0845 system. The original OSIRIS image (O) is shown on the top-left plot. The dashed lines, parallel to each other, indicate the limits introduced to reconstruct the PSF. The best reconstructed images of the secondary (<P2>) and primary (<P1>) are displayed in the top-right and bottom-right plots with their centroid marked with a cross. The difference between the intensities of the secondary and the primary (red crosses), after being scaled by the flux ratio and shifted to the position of the secondary is illustrated in the bottom-left plot. The box shows the region where the  $\chi^2$  statistics are calculated.

mutual flux contamination between the two sources. Note the sum of <P1> and <P2> is exactly O ( $\equiv$  <P1> + <P2>), so we separate the original reduced image into two different components. We finally shift <P1>, multiply by  $\gamma$ , to the position of <P2> and then calculate the residuals.

We explore the parameter space to find the best solution, i.e. the one with the smallest value of  $\chi^2$  in the OSIRIS images. We also repeated the procedure on the individual sky-corrected NIRC2 images (right panel in Fig. 4). We illustrate the method applied to separate the point-like sources of both binaries in the left-hand side of Fig. 3. We show the decomposition of the best solution for UGCS0845 and UGCS0830 in the right panel of Fig. 3 and in Fig. 4, respectively. We sample the parameter space in steps of 0.1 pixel, 3 degrees, and 0.05 for the zero points, positions, angle, and flux ratio, respectively. For the best solution, we derive the centroids of every source, using the flux values above 50% of the peak. The positions of the two centroids were employed to determine the separation and the position angle of the nodes corresponding to the binary components. We also determine the FWHM of the reconstructed PSF. In every case we used the best five images, deriving the mean and standard deviation values of each output parameter.

#### 4.2 Physical separation and orientation

We apply this method to four blocks of individual OSIRIS images independently: one block taken on 20 November 2018 and three collected on 24 January 2019. We measure consis-

tent separations of 6.28, 5.92, 6.08, and 6.00 pixels for the four images, given us the confidence that UGCS0845 is a binary with a median projected separation of  $6.07 \pm 0.13$  pixels ( $1\sigma$ ).

Adopting the plate scale of  $9.9407 \pm 0.0071$  mas measured in Section 3 for OSIRIS, we derive a mean physical separation of  $60.3 \pm 1.3$  mas with a position angle of  $295 \pm 1.5$  degrees from North to East anti-clockwise, and a flux ratio of  $0.89 \pm 0.04$  (Fig. 4). This corresponds to a projected physical separation of  $11.2 \pm 0.7$  au, assuming a distance of 186.18 pc and a dispersion of 10.7 pc for Praesepe (Table 1). The error bars quoted on angular separations measured in mas take into account the dispersion of the astrometric determinations plus the uncertainty of the pixel size determination.

Our method is able to separate the two components of the binary, which we barely resolve. The diffraction limit of Keck/OSIRIS corresponds to 5 pixels and a FWHM of  $\sim 7$  pixels can be achieved in the best conditions (e.g. Liu et al. 2008; Dupuy & Liu 2012). Our method gives a FWHM of  $7.7 \pm 0.8$  pixels. Given the consistency obtained for the separations derived from four independent images and the similar elongation between the stacked images collected in November 2018 and January 2019, we are confident that the results are reliable even though AO images often suffer from uncontrolled systematics.

We apply the same procedure to the OSIRIS images of UGCS0830. We separate the two components into a binary with a flux ratio of  $0.49 \pm 0.07$  ( $1\sigma$ ) and a projected separation of  $6.23 \pm 0.26$  pixels ( $1\sigma$ ) equivalent to  $61.9 \pm 2.6$  mas and

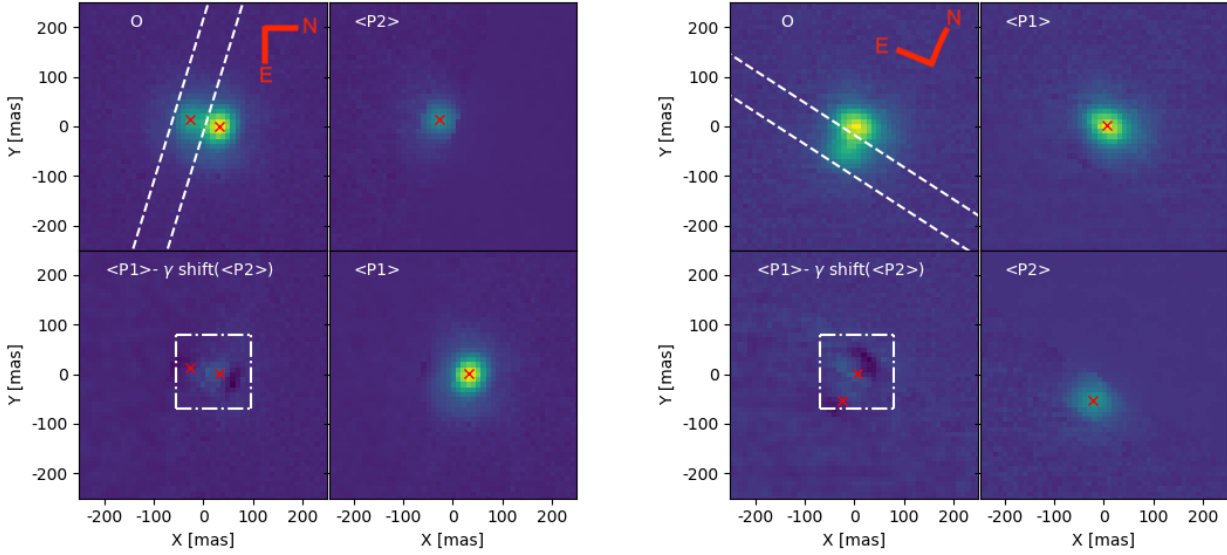


**Figure 4.** *Left panel:* *Top-left:* Reduced OSIRIS image of UGCS0830 (O). The dashed lines, parallel to each other, indicate the limits introduced to reconstruct the PSF of the UGCS0830 system. *Top-right:* Best reconstructed image of the secondary (<P2>) and its centroid marked with a red cross. *Bottom-right:* Best reconstructed image of the primary (<P1>) and its centroid marked with a red cross. *Bottom-left:* Difference between the intensities of the secondary and the primary, after being scaled by the flux ratio and shifted to the position of the secondary. The positions of P1 and P2 are marked with red crosses. The white box shows the region where the  $\chi^2$  statistics are calculated. *Right panel:* Same as left panel but for the NIRC2 images of UGCS0830. We indicate the orientation of the detector with respect to North and East.

corresponding to a physical separation of  $11.5 \pm 0.8$  au (Fig. 4). We measured the orientation of the binary on the image of  $73 \pm 4$  degrees, corresponding to a position angle of  $197 \pm 4$  degrees.

We repeated the measurements for the NIRC2 images of UGCS0830. We selected the best five images to infer a flux ratio of  $0.46 \pm 0.03$ , separation of  $6.27 \pm 0.09$  pixels ( $1\sigma$ ) equivalent to  $62.5 \pm 0.9$  mas. We measured an angle of  $150.4 \pm 1.2$  degrees on the image, translating into an position angle of  $180.4 \pm 1.2$  degrees. The quoted error bars stand for the dispersion of the measurements on the selected individual images. In Table 1, we give the measurements at  $1\sigma$  for both instruments.

We caution, however, that the angular separation may be underestimating the true projected separation of the binary. Indeed, the two components of UGCS0830 are close and the significantly different brightness of the two members artificially makes the centroid of the secondary shift towards the position of the primary. The position angle should not be affected significantly but the flux ratio and separation are. Nonetheless, we observe that the position angles measured on both instruments for UGCS0830 differ by 16–17 degrees.

Despite the excellent agreement in the separation and flux between the two instruments, the position angle differs. At this stage, we fail to reconcile the position angles of UGCS0830 derived from two sets of observations with two different instruments. We discuss possible reasons for such difference. (i) The binary might show a significant orbital motion, which may hint at a very elliptical orbit, or its true separation is smaller than the projected separation creating a shorter orbital period. However, we do not observe a sig-

nificant change in the separation of both components. We conclude that further observations are needed to confirm or not this possible orbital motion. (ii) The LGS-AO observations suffered from uncontrolled problems although this hypothesis is not supported by the good quality of the images of the tip-tilt star observed just before our targets. The AO correction of both datasets is of good quality. (iii) The determination of the position angles using our method (Section 4.1) might suffer from uncontrolled systematics, but the determination of the angles with our method is robust and confirmed on individual images as well as with telescope offsets in the headers. (iv) The companion candidate might be an unrelated field/background source. Considering the separations of 61.9 mas and 62.5 mas on 11 March 2019 and 22 March 2020 (i.e. slightly less than 1 year apart), the change in position angle from 197 degrees to 180 degrees could be interpreted as a relative proper motion of the companion candidate relative to UGCS0830 of  $+18.3 \pm 5.2$  mas/yr and  $-3.4 \pm 3.9$  mas/yr in right ascension and declination, respectively. Hence, the proper motion of the possible companion would be  $(-9.3 \pm 7.3, -9.9 \pm 6.3)$  mas/yr,  $2\sigma$  away from the proper motion of UGCS0830 ( $(-27.6 \pm 4.9, -6.5 \pm 4.9)$  mas/yr; Boudreault et al. 2012; Lawrence et al. 2013). Furthermore, the proper motion of the companion lies within  $3\sigma$  of the mean motion of Praesepe ( $(-34.2 \pm 2.7, -7.4 \pm 4.2)$  mas/yr; Boudreault et al. 2012), thus, cannot be totally discarded as a probable member. We have also computed the probability of finding a source fainter than UGCS0830 ( $K = 16.5$  mag) and as faint as the companion candidate ( $K = 17.5$  mag) within 1 arcsec from UGCS0830. We estimated the density of objects selecting all point-like and extended sources in

the UKIDSS GCS database in an area of  $1 \text{ deg}^2$  centered around UGCS0830. We find 4075 satisfying those criteria, translating into a probability of chance alignment of  $10^{-3}$ . This estimate is an upper limit because the companion candidate lies at about 62 mas, implying a lower probability of chance alignment of  $3.8 \times 10^{-6}$ . We conclude that the likelihood that both UGCS0830 and the possible companion are not physically bound is extremely small.

### 4.3 Spectral type

UGCS0845 was classified as an  $L0.4 \pm 0.3$  dwarf (equivalent to an effective temperature of  $2279 \pm 371 \text{ K}$ ) comparing its GTC/OSIRIS low-resolution optical spectrum with M and L dwarf templates observed with the same instrumentation and inferring spectral indices, see Boudreault & Lodieu (2013) for a detailed description of the method. We revise the spectral classification here, classifying the unresolved system in the optical and near-infrared independently. We classify the UGCS0845 system as an  $L1.0 \pm 0.5$  dwarf (Table 1) by direct comparison with Sloan optical spectra of old high-gravity L dwarfs (Schmidt et al. 2010) as shown in the left-hand side panel of Fig. 2. We classify the system as an L1.5 dwarf in the near-infrared because the VLT/X-shooter spectrum is best fitted by the SpeX spectrum of 2MASS J14182962–3538060 (right-hand side panel of Fig. 2) classified as a field L1.5 dwarf by Kirkpatrick et al. (2010)<sup>2</sup>. This spectral type agree with the one obtained in Manjavacas et al. (2020). Hence, we conclude that the full spectral energy distribution of UGCS0845 is most consistent with an  $L1.0$ – $L1.5 \pm 0.5$  dwarf, slightly later than the original classification. According to the polynomials for old field M6–T9 dwarfs defined by Filippazzo et al. (2015), we infer a mean effective temperature of 2030–2100 K for the system with an rms of 113 K. Similar effective temperatures ( $2200 \pm 100 \text{ K}$ ) are derived from the spectral types-effective temperature relations of Golimowski et al. (2004) and Vrba et al. (2004). Because UGCS0845 is an almost equal-flux binary, we would expect the primary and secondary to have very similar spectral types around L1.0.

We did not collect a spectrum for UGCS0830 but its position in the colour-magnitude diagrams (Fig. 1) suggests that it is of later spectral type than UGCS0845. Indeed, UGCS0830 appears fainter in  $K$ -band magnitudes than UGCS0845 and also harbours a redder  $Y - K$  colour. In Section 4.4, we infer luminosity intervals for each component of UGCS0830. Using the luminosity-spectral type relation of Filippazzo et al. (2015) valid for old field M6–T9 dwarfs, we estimate spectral types of M9–L1 and L3–L5 for the primary and secondary of UGCS0830, respectively (Table 1).

### 4.4 Bolometric luminosity

We integrate the spectral energy distribution of the UGCS0845 unresolved system using photometry from the three distinct public surveys (Table 2): the  $riz$  magnitudes from the Sloan Digital Sky Survey DR12 (Alam et al. 2015), the  $ZYJHK$  magnitudes from the UKIDSS Galactic Clusters Survey (Lawrence et al. 2007), and the AllWISE survey

(Wright et al. 2010; Cutri & et al. 2014). We complement the photometry with the spectrum of the BT-Settl model at a temperature of 2100 K (with solar-metallicity and gravity of  $\log(g) = 5.0$  dex) to estimate fluxes in the blue (negligible for these objects below 300 nm) and the red part of the spectral energy distribution (about 50% beyond 5 microns). We derive a total (i.e. for the unresolved system) photometric bolometric luminosity of  $5.616 \times 10^4 \text{ erg/s}$  for UGCS0845, yielding  $\log(L/L_\odot) = -3.25 \pm 0.03$  dex, assuming a distance of 186.18 pc. The depth of the cluster taken as the tidal radius adds a non-negligible error budget of 0.06 dex, yielding  $\log(L/L_\odot) = -3.25 \pm 0.07$  dex (Table 1).

We also estimate the bolometric luminosity of UGCS0845 by integrating the full flux-calibrated optical and near infrared spectrum, and the  $W1$  and  $W2$  photometry in the mid-infrared. We calibrate in flux the optical and the near-infrared spectra independently, using the  $z$ -Pan-Starrs and the  $J$ -UKIDSS photometry, respectively. To obtain the bolometric luminosity, we integrate the full spectral energy distribution from 0 to 1000 microns, interpolating the gaps between the available optical and near-infrared spectra, and photometric points with their associated errors by performing a linear interpolation (see Manjavacas et al. 2020). We find  $\log(L/L_\odot) = -3.24 \pm 0.09$  dex, in agreement with the photometric value. Given the flux ratio of 0.89 with an uncertainty of 0.04, which translates into an additional budget uncertainty of 0.02 dex, we infer luminosities of  $\log(L/L_\odot) = -3.49 \pm 0.09$  dex and  $-3.60 \pm 0.09$  dex for the primary and secondary, respectively (Table 1), adopting equal spectral energy distribution as reasonable approximation for UGCS0845. A more accurate distance for the binary system would significantly decrease the uncertainty on the luminosities and, more importantly, on the masses but *Gaia* data are not available for our sources.

We have only photometry for UGCS0830 (Table 2) so we integrate the spectral energy distribution of the unresolved system using photometry from Sloan, UKIDSS GCS, and AllWISE, as for UGCS0845. We infer a system bolometric luminosity of  $\log(L/L_\odot) = -3.44 \pm 0.08$  dex. Given our adopted flux ratio of  $0.46 \pm 0.03$ , we infer luminosities of  $\log(L/L_\odot) = -3.60 \pm 0.08$  dex and  $-3.94 \pm 0.10$  dex for the primary and secondary, respectively. We note that we did not take into account the difference in  $K$ -band bolometric correction between the primary and secondary components of UGCS0830 that can reach up to 0.2 mag between a field M9 and L5 dwarf (Filippazzo et al. 2015).

### 4.5 Masses

#### 4.5.1 UGCS0845

We derive the masses from the total bolometric luminosity calculated from the full spectral energy distribution using the latest BT-Settl isochrones (Baraffe et al. 2015). For a flux ratio of 0.76 and a mean age of 700 Myr, we infer masses of  $0.078 M_\odot$  and  $0.073 M_\odot$  for the primary and secondary, respectively (Table 3). The uncertainty of 0.07 dex in  $\log(L/L_\odot)$ , which does not include the uncertainty in the differing spectral energy distributions, translates approximately into a (formal) uncertainty of at most  $0.002 M_\odot$  on the mass. We show the full range of values taking into account all uncertainties on flux ratio and age in Table 3.

<sup>2</sup> Spectrum publicly available at <http://pono.ucsd.edu/~adam/>

**Table 1.** Main parameters of the two binary systems in the Praesepe open cluster presented in this work.  $1\sigma$  error bars. <sup>a</sup>: Parameters from OSIRIS; <sup>b</sup>: Parameters from NIRC2. <sup>c</sup>: UGCS0845 was also observed on 2458507 and 2458563. <sup>d</sup>: system luminosity.

Name	BJD days	SpT	Separation mas	Separation au	PA deg	Flux ratio	$\Delta K$ mag	Period year	$\log(L/L_{\odot})$ dex
UGCS0845 <sup>a</sup>	2458442 <sup>c</sup>	L1.0±0.5	60.3±1.3	11.2±0.7	295.0±1.5	0.89±0.04	0.13±0.05	96.8±9.0	-3.24±0.09 <sup>d</sup>
UGCS0830 <sup>a</sup>	2458564	—	61.9±2.6	11.5±0.8	197.0±4.0	0.49±0.07	0.77 <sup>+0.17</sup> <sub>-0.15</sub>	110.4±11.9	-3.44±0.08 <sup>b</sup>
UGCS0830 <sup>b</sup>	2458918	—	62.5±0.9	11.6±0.7	180.4±1.2	0.46±0.03	0.84±0.07	109.7±10.5	-3.44±0.08 <sup>b</sup>

**Table 2.** Photometry of the unresolved systems from Pan-Starrs Data release 1 (Chambers et al. 2016), Sloan (Alam et al. 2015) in the AB system (Fukugita et al. 1996), UKIDSS Galactic Clusters Survey (GCS) (Lawrence et al. 2007) in the Mauna Kea Vega system (Tokunaga et al. 2002), and AllWISE (Cutri & et al. 2014) in the Vega system.

Filter	UGCS0845	UGCS0830
PS1 <i>i</i>	21.536±0.044	21.676±0.147
PS1 <i>z</i>	20.324±0.054	20.682±0.043
PS1 <i>y</i>	19.311±0.051	19.842±0.060
SDSS DR12 <i>r</i>	23.934±0.443	23.823±0.619
SDSS DR12 <i>i</i>	21.878±0.150	21.656±0.141
SDSS DR12 <i>z</i>	19.954±0.105	20.116±0.145
UKIDSS GCS <i>Z</i>	19.783±0.131	19.923±0.099
UKIDSS GCS <i>Y</i>	18.376±0.055	19.076±0.066
UKIDSS GCS <i>J</i>	17.419±0.033	17.868±0.040
UKIDSS GCS <i>H</i>	16.689±0.023	17.115±0.041
UKIDSS GCS <i>K</i>	16.033±0.024	16.512±0.048
AllWISE <i>w1</i>	15.647±0.048	16.146±0.086
AllWISE <i>w2</i>	15.318±0.115	15.909±0.222

Assuming ages of 600 Myr and 800 Myr for Praesepe, the masses would change by  $0.002 M_{\odot}$ . In the case of flux ratios of 0.85 and 0.93, the formal differences in the masses of the primary and the secondary is below one Jupiter mass (Table 3). We have also included the masses for an upper limit of 1 Gyr on the age of Praesepe.

In all cases, the secondary straddles the stellar/substellar boundary ( $0.072\text{--}0.076 M_{\odot}$ ) and might be either a very low-mass star or a brown dwarf depending on the age adopted for the cluster, while the primary would be a very low-mass star ( $0.074\text{--}0.078 M_{\odot}$ ) just above the hydrogen-burning limit set to  $0.072 M_{\odot}$  at solar metallicity (Chabrier & Baraffe 1997).

To obtain an independent estimate of the mass of the system with the lithium test in a similar-aged cluster such as the Hyades, we have compared the magnitudes of UGCS0845 with the very low mass stars and brown dwarfs confirmed spectroscopically in the Hyades open cluster ( $d = 47.50 \pm 0.15$  pc; Gaia Collaboration et al. 2018b) whose age is comparable to Praesepe (600–750 Myr; Maeder & Mermilliod 1981; Mermilliod 1981; Mazzei & Pigatto 1988; De Gennaro et al. 2009; Lebreton et al. 2001; Brandt & Huang 2015b; Martín et al. 2018; Lodieu et al. 2018b). Among the 12 L dwarfs identified in the Hyades by Hogan et al. (2008), ten of them were confirmed spectroscopically as members (Lodieu et al. 2014), including three brown dwarfs with masses below  $0.06 M_{\odot}$  with lithium in absorption at  $6707.8 \text{ \AA}$  (Martín et al. 2018). The lithium depletion boundary in the Hyades is located at  $M_J = 12.2\text{--}12.7$  mag and  $M_K = 10.8\text{--}10.9$  mag, respectively.

The absolute magnitudes of UGCS0845 are  $M_J = 11.07 \pm 0.10$  and  $M_K = 9.68 \pm 0.11$  mag, where the uncertainty take into account the depth of the cluster (Table 2).

In the case of a system with the secondary having 0.89 times the flux of the primary, the magnitudes of the primary and secondary would be  $M_K = 10.38 \pm 0.05$  mag and  $M_K = 10.50 \pm 0.09$  mag, respectively.

According to the latest BT-Settl models (Baraffe et al. 2015), the hydrogen-burning limit is 1.0 mag and 0.6 mag brighter than the lithium depletion boundary in the *J*- and *K*-band, respectively, at an age of 600 Myr (1.1 and 0.8 mag at 700 Myr), suggesting that the primary might be a star and the secondary a high-mass brown dwarf. Hence, we do not expect a strong lithium abundance for high-mass brown dwarfs because they will most likely have depleted most of the original lithium at the age of the cluster. However, if we can detect a tiny fraction of lithium in the spectrum of the secondary, it will be very important to constrain the masses, evolutionary models and even Li destruction models when dynamical masses are in hands.

Applying the Kepler’s third law, we infer an orbital period of  $96.8 \pm 9.0$  years, assuming total mass of  $0.150 \pm 0.004 M_{\odot}$  and zero eccentricity (Table 1).

#### 4.5.2 UGCS0830

We derive the masses from the total bolometric luminosity calculated from the photometry using the BT-Settl isochrones. For a flux ratio of 0.46 and a mean age of 700 Myr, we infer masses of  $0.073 M_{\odot}$  and  $0.059 M_{\odot}$  for the primary and secondary, respectively (Table 3). The uncertainty of 0.03 dex in  $\log(L/L_{\odot})$  translates approximately into a (formal) uncertainty of at most  $0.002 M_{\odot}$  on the mass. Repeating the procedure for the 600–800 Myr range of possible ages for Praesepe (Table 3), we infer masses close to or above the hydrogen-burning limit for the primary ( $0.070\text{--}0.078 M_{\odot}$ ) and in the substellar regime for the secondary ( $0.051\text{--}0.065 M_{\odot}$ ), implying that it would be the first brown dwarf discovered in the Praesepe with L spectral type for which a precise dynamical mass can be derived in the next decades. If Praesepe is 1 Gyr-old, the masses of the primary and secondary of UGCS0830 could be as high as  $0.078$  and  $0.066 M_{\odot}$ , respectively.

We also performed the computation taking the Hyades as a reference, as for UGCS0845. We inferred an absolute *K*-band magnitude of  $M_K = 10.16 \pm 0.08$  mag for UGCS0830. If we split the system into a binary with a flux ratio of 0.46, we infer absolute magnitudes of  $M_K = 10.573^{+0.199}_{-0.192}$  mag and  $11.415^{+0.295}_{-0.245}$  mag for the primary and secondary, respectively, taking into account the depth of the cluster and propagating uncertainty on the photometry and flux ratio.



**Table 3.** Masses of each component of the UGCS0845 (top two rows) system as a function of the flux ratio ( $0.89 \pm 0.04$ ) and the age assumed for Praesepe (600, 700, and 800 Myr) with an upper limit of 1 Gyr. The formal uncertainty on each mass estimate is of the order of  $0.001 M_{\odot}$ . We list the masses of each component of UGCS0830 for the adopted flux ratio and the age range of the cluster in the bottom two rows.

Age (Myr)	600			700			800			1000		
Flux ratio	0.85	0.89	0.93	0.85	0.89	0.93	0.85	0.89	0.93	0.85	0.89	0.93
$M_{\text{prim}} (M_{\odot})$	0.074	0.074	0.074	0.076	0.076	0.076	0.078	0.078	0.078	0.080	0.080	0.080
$M_{\text{sec}} (M_{\odot})$	0.072	0.072	0.072	0.074	0.074	0.074	0.076	0.076	0.076	0.078	0.078	0.078
Age (Myr)	600			700			800			1000		
Flux ratio	0.43	0.46	0.49	0.43	0.46	0.49	0.43	0.46	0.49	0.43	0.46	0.49
$M_{\text{prim}} (M_{\odot})$	0.071	0.071	0.070	0.074	0.073	0.073	0.076	0.075	0.078	0.078	0.077	0.077
$M_{\text{sec}} (M_{\odot})$	0.051	0.055	0.056	0.058	0.059	0.060	0.061	0.063	0.065	0.066	0.067	0.067

Hence, the primary is expected to be a massive brown dwarf whose lithium has been depleted while the secondary is a brown dwarf at the lithium depletion boundary. For a brown dwarf that has fully retained its lithium, we expect a pseudo-equivalent widths in the 6–20 Å range (Kirkpatrick et al. 2000, 2008; Cruz et al. 2009; Martín et al. 2018; Lodieu et al. 2018b). Taking into account the dilution factor due to the fact that the primary should not exhibit lithium in absorption, we would expect a system pseudo-equivalent width of 1.0–7.6 Å for the lithium absorption line at 6707.8 Å in the integrated optical spectrum of the system.

Applying the Kepler’s law, we infer an orbital period of  $109.7 \pm 12.4$  years, assuming zero eccentricity and a total mass of  $0.132 \pm 0.008 M_{\odot}$  (Table 1).

## 5 DISCUSSION

We have confirmed the binarity of UGCS0845 and a companion candidate to UGCS0830. In this discussion, we assume that both are true binaries. Both systems represent the first binaries across the hydrogen-burning limit in Praesepe and the first L–L binaries in this cluster. Many surveys referenced throughout this work have screened low-mass stars and brown dwarfs for companions in clusters younger than 700 Myr, but only L–L binaries have been reported in the Hyades so far. These new systems represent important discoveries to measure dynamical masses across the hydrogen-burning limit and in the substellar regime, locate the lithium depletion boundary, provide an estimation of the multiplicity properties of low-mass stars and brown dwarfs at a given age, and constrain stellar evolutionary models in a mass regime where physics is complex (Baraffe et al. 2015).

We plot the H–R diagram of Praesepe in Fig. 5 showing all members within the tidal radius of the cluster identified in *Gaia* DR2 (Lodieu et al. 2019) with the location of the components of the two binaries presented in this work. We observe that they lie across the hydrogen-burning limit based on model predictions (Baraffe et al. 2015) and have spectral types later than M9/L0 according to the field relation of Pecaut & Mamajek (2013). We have only the  $K$ -band magnitude difference for both systems so we assumed the  $J - K$  colour of the system for each component of UGCS0845 because the almost equal flux ratio. In the case of UGCS0830,

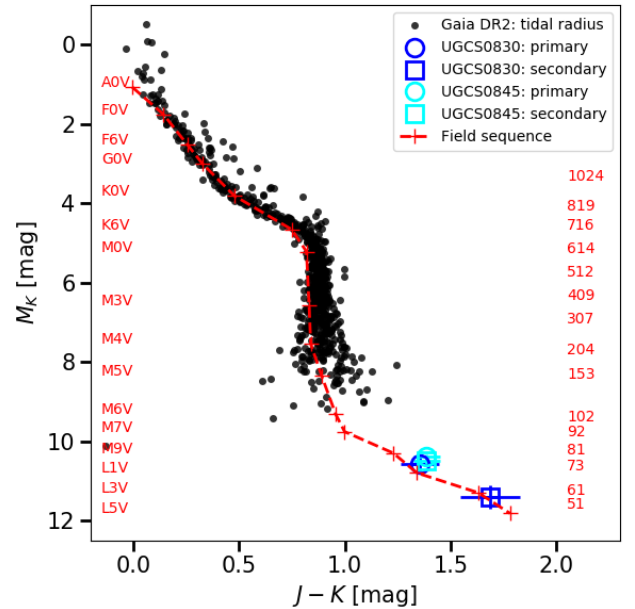


**Figure 5.** Hertzsprung-Russell diagram for Praesepe. We plot cluster members from *Gaia* DR2 within the tidal radius (Lodieu et al. 2019) as black dots. We overplot the position of each component of UGCS0845 and UGCS0830 in cyan and blue, respectively. We added an estimate of the spectral type from the absolute magnitude-spectral relation of field dwarfs (Pecaut & Mamajek 2013) and masses predicted by the BT-Settl models for an age of 700 Myr (Baraffe et al. 2015).

we assume the colour of a L3 dwarf for the secondary and included an additional error of  $+0.1$  mag to take into account the lack of spectral type. These two binaries represent important to extend the Praesepe sequence into the substellar regime with future deep surveys.

Boudreault et al. (2012) estimated a photometric multiplicity of  $23.2 \pm 5.6\%$  in the  $0.4 - 0.1 M_{\odot}$  mass range. This is comparable to the frequency of Hyades low-mass stars and brown dwarfs derived early on by Gizis & Reid (1995) with a fraction of  $27 \pm 16\%$  and later by Duchêne et al. (2013) who resolved 3 out of 16 targets with adaptive optics ( $19^{+13}_{-6}\%$  in 2–350 au). However, this estimate should be revised because

one of the resolved system (Hya05) was rejected as a spectroscopic member of the Hyades (Lodieu et al. 2014), yielding a lower multiplicity of  $\sim 13.3\%$  (2/15). The binary sequence of Praesepe is well seen in various colour-magnitude diagrams and fitted by a red line in Fig. 1. We confirm two of the photometric binary candidates with adaptive optics, suggesting that the multiplicity of  $23.2 \pm 5.6\%$  estimated by Boudreault et al. (2012) for the  $0.1\text{--}0.07 M_{\odot}$  range may hold, if all photometric and astrometric candidates are later confirmed as spectroscopic members. This photometric binary fraction agrees with the overall multiplicity fraction of field brown dwarfs (18–28% Duchêne & Kraus 2013) and is also consistent with the theoretical predictions of hydrodynamical simulations ( $27.3 \pm 11.6\%$ ; Bate 2012).

For comparable mass intervals but younger ages, where multiplicity fractions remain very uncertain, we should highlight some key results. Considering current uncertainties sample sizes, those comparisons should be taken with a pinch of salt but necessary to understand the evolution of multiple systems with age. In the Pleiades, whose age is around 125 Myr (Stauffer et al. 1998; Barrado y Navascués et al. 2004), Martín et al. (2003) and Bouy et al. (2006b) derived a binary fraction of 9–27% for separations larger than 7 au and mass ratios greater than 0.45–0.9 based on a sample of 15 substellar members with spectral types in the M6–M9 range ( $0.055\text{--}0.065 M_{\odot}$ ). At younger ages (i.e. star-forming regions younger than about 10 Myr), there might be a trend for a sharp decrease from 15–28% for very low-mass stars ( $0.15\text{--}0.07 M_{\odot}$ ) down to less than 11% (50% confidence) below  $0.1 M_{\odot}$  (Kraus & Hillenbrand 2012; Duchêne & Kraus 2013). The latter is consistent with the 3–7% of binaries imaged in a sample of  $>100$  young M6 dwarfs and later type in Taurus and Chamaeleon (Todorov et al. 2014). The binary fraction of brown dwarfs in Praesepe might not be primordial but affected by dynamical evolution of the cluster.

## 6 CONCLUSIONS AND FUTURE PLANS

We report two new ultracool binary systems composed of two L dwarfs straddling the stellar/substellar in the Praesepe open cluster. Both systems have projected separations of about 60 mas, corresponding to physical separations of  $\sim 11\text{--}12$  au and minimum orbital periods of approximately 100 years. If confirmed as a companion, the secondary of the system with the largest flux ratio lies unambiguously in the brown dwarf regime, and we argue that the lithium feature should be present in absorption at  $6707.8 \text{ \AA}$ . Both systems are key to locate with higher precision the position of the stellar/substellar and lithium depletion boundaries in Praesepe. If the photometric multiplicity among Praesepe members with masses below the hydrogen-burning limit holds, we argue that the binary fraction in Praesepe might not be primordial.

We plan to continue the follow-up of these two binaries with the LGS systems on Keck and the future AO laser guide star system on the Gran Telescopio de Canarias (GTCAO-LGS; Béjar et al. 2019) and the FRIDA instrument (inFRared Imager and Dissector for Adaptive optics; Watson et al. 2016) for the next decade to derive dynamical masses of both components and measure the amount of lithium in each component. The accuracy of these dynamical masses

will depend on the evolution of the separation of the system with time, i.e. whether we observed the system at periastron or not. The upcoming HARMONI spectrograph (High Angular Resolution Monolithic Optical & Near-infrared Integral field; Tecza et al. 2009; Thatte et al. 2010) on the extremely large telescope should provide us with better spatial resolution and sensitivity to monitor their orbits.

## ACKNOWLEDGEMENTS

NL and VJSB were supported by the Spanish Ministry of Economy and Competitiveness (MINECO) under the grants AYA2015-69350-C3-2-P. CdB acknowledges the funding of his sabbatical position through the Mexican national council for science and technology (CONACYT grant CVU No. 448248). He is also thankful for the support from the Jesus Serra Foundation Guest Program. MRZO was supported by MINECO grant number AYA2014-54348-C3-2-R. The data presented herein were obtained at the W. M. Keck Observatory, which is operated as a scientific partnership among the California Institute of Technology, the University of California and the National Aeronautics and Space Administration. The Observatory was made possible by the generous financial support of the W. M. Keck Foundation. The authors wish to recognise and acknowledge the very significant cultural role and reverence that the summit of Maunakea has always had within the indigenous Hawaiian community. We are most fortunate to have the opportunity to conduct observations from this mountain.

Based on observations made with ESO Telescopes at the La Silla Paranal Observatory under programme ID 098.C-0277(A), PI Manjavacas. This work is based on observations (programme GTC66-12B; PI Boudreault) made with the Gran Telescopio Canarias (GTC), operated on the island of La Palma in the Spanish Observatorio del Roque de los Muchachos of the Instituto de Astrofísica de Canarias. This research has made use of the Simbad and Vizier (Ochsenbein et al. 2000) databases, operated at the Centre de Données Astronomiques de Strasbourg (CDS), and of NASA’s Astrophysics Data System Bibliographic Services (ADS).

This work has made use of data from the European Space Agency (ESA) mission *Gaia* (<https://www.cosmos.esa.int/gaia>), processed by the *Gaia* Data Processing and Analysis Consortium (DPAC, <https://www.cosmos.esa.int/web/gaia/dpac/consortium>). Funding for the DPAC has been provided by national institutions, in particular the institutions participating in the *Gaia* Multilateral Agreement. Funding for the Sloan Digital Sky Survey IV has been provided by the Alfred P. Sloan Foundation, the U.S. Department of Energy Office of Science, and the Participating Institutions. SDSS-IV acknowledges support and resources from the Center for High-Performance Computing at the University of Utah. The SDSS web site is [www.sdss.org](http://www.sdss.org). SDSS-IV is managed by the Astrophysical Research Consortium for the Participating Institutions of the SDSS Collaboration including the Brazilian Participation Group, the Carnegie Institution for Science, Carnegie Mellon University, the Chilean Participation Group, the French Participation Group, Harvard-Smithsonian Center for Astrophysics, Instituto de Astrofísica de Canarias, The Johns Hopkins University, Kavli Institute for the Physics

and Mathematics of the Universe (IPMU) / University of Tokyo, Lawrence Berkeley National Laboratory, Leibniz Institut für Astrophysik Potsdam (AIP), Max-Planck-Institut für Astronomie (MPIA Heidelberg), Max-Planck-Institut für Astrophysik (MPA Garching), Max-Planck-Institut für Extraterrestrische Physik (MPE), National Astronomical Observatory of China, New Mexico State University, New York University, University of Notre Dame, Observatório Nacional / MCTI, The Ohio State University, Pennsylvania State University, Shanghai Astronomical Observatory, United Kingdom Participation Group, Universidad Nacional Autónoma de México, University of Arizona, University of Colorado Boulder, University of Oxford, University of Portsmouth, University of Utah, University of Virginia, University of Washington, University of Wisconsin, Vanderbilt University, and Yale University.

Based on data from the UKIRT Infrared Deep Sky Survey (UKIDSS). The UKIDSS project is defined in [Lawrence et al. \(2007\)](#) and uses the UKIRT Wide Field Camera (WFCAM; [Casali et al. 2007](#)). The photometric system is described in [Hewett et al. \(2006\)](#) and the calibration is described in [Hodgkin et al. \(2009\)](#). The pipeline processing and science archive are described in Irwin et al. (in prep) and [Hambly et al. \(2008\)](#).

This publication makes use of data products from the Wide-field Infrared Survey Explorer, which is a joint project of the University of California, Los Angeles, and the Jet Propulsion Laboratory/California Institute of Technology, and NEOWISE, which is a project of the Jet Propulsion Laboratory/California Institute of Technology. WISE and NEOWISE are funded by the National Aeronautics and Space Administration.

**Data Availability Statement** The data underlying this article will be shared on reasonable request to the corresponding author.

## REFERENCES

- Adams T., Davies M. B., Jameson R. F., Scally A., 2002, *MNRAS*, **333**, 547
- Ahmic M., Jayawardhana R., Brandeker A., Scholz A., van Kerkwijk M. H., Delgado-Donate E., Froebrich D., 2007, *ArXiv e-prints*, 0708.3851, 708
- Alam S., et al., 2015, *ApJS*, **219**, 12
- Allers K. N., et al., 2009, *ApJ*, **697**, 824
- Arriaga P., Fitzgerald M., Johnson C., Weiss J., Lyke J. E., 2018, in *Ground-based and Airborne Instrumentation for Astronomy VII*. p. 107022U, [doi:10.1117/12.2313101](#)
- Artigau É., Gagné J., Faherty J., Malo L., Naud M.-E., Doyon R., Lafrenière D., Beletsky Y., 2015, *ApJ*, **806**, 254
- Baker D. E. A., Jameson R. F., Casewell S. L., Deacon N., Lodieu N., Hambly N., 2010, *MNRAS*, **408**, 2457
- Baraffe I., Homeier D., Allard F., Chabrier G., 2015, *A&A*, **577**, A42
- Barrado y Navascués D., Stauffer J. R., Jayawardhana R., 2004, *ApJ*, **614**, 386
- Bate M. R., 2012, *MNRAS*, **419**, 3115
- Béjar V. J. S., Zapatero Osorio M. R., Pérez-Garrido A., Álvarez C., Martín E. L., Rebolo R., Villó-Pérez I., Díaz-Sánchez A., 2008, *ApJL*, **673**, L185
- Béjar V. J. S., et al., 2019, in Montesinos B., Asensio Ramos A., Buitrago F., Schödel R., Villaver E., Pérez-Hoyos S., Ordóñez-Etxeberria I., eds, *Highlights on Spanish Astrophysics X*. pp 536–541
- Billar B., Allers K., Liu M., Close L. M., Dupuy T., 2011, *ApJ*, **730**, 39
- Boudreault S., Lodieu N., 2013, *MNRAS*, **434**, 142
- Boudreault S., Bailer-Jones C. A. L., Goldman B., Henning T., Caballero J. A., 2010, *A&A*, **510**, A27
- Boudreault S., Lodieu N., Deacon N. R., Hambly N. C., 2012, *MNRAS*, **426**, 3419
- Bouy H., Brandner W., Martín E. L., Delfosse X., Allard F., Baraffe I., Forveille T., Demarco R., 2004, *A&A*, **424**, 213
- Bouy H., Martín E. L., Brandner W., Zapatero-Osorio M. R., Béjar V. J. S., Schirmer M., Huélamo N., Ghez A. M., 2006a, *A&A*, **451**, 177
- Bouy H., Moraux E., Bouvier J., Brandner W., Martín E. L., Allard F., Baraffe I., Fernández M., 2006b, *ApJ*, **637**, 1056
- Brandt T. D., Huang C. X., 2015a, *ApJ*, **807**, 24
- Brandt T. D., Huang C. X., 2015b, *ApJ*, **807**, 58
- Burgasser A. J., 2007, *ApJ*, **658**, 617
- Burgasser A. J., McElwain M. W., 2006, *AJ*, **131**, 1007
- Burgasser A. J., Reid I. N., Siegler N., Close L., Allen P., Lowrance P., Gizis J., 2007, in Reipurth B., Jewitt D., Keil K., eds, *Protostars and Planets V*. pp 427–441
- Casali M., Adamson A., Alves de Oliveira C., Almaini O., Burch K., Chuter T., Elliot J., 23 co-authors 2007, *A&A*, **467**, 777
- Cepa J., et al., 2000, in M. Iye & A. F. Moorwood ed., *Society of Photo-Optical Instrumentation Engineers (SPIE) Conference Series Vol. 4008*, Society of Photo-Optical Instrumentation Engineers (SPIE) Conference Series. pp 623–631
- Chabrier G., Baraffe I., 1997, *A&A*, **327**, 1039
- Chambers K. C., Magnier E. A., Metcalfe N., 103 co-authors 2016, *ApJ*,
- Chappelle R. J., Pinfield D. J., Steele I. A., Dobbie P. D., Magazzù A., 2005, *MNRAS*, **361**, 1323
- Chauvin G., Lagrange A.-M., Dumas C., Zuckerman B., Mouillet D., Song I., Beuzit J.-L., Lowrance P., 2005, *A&A*, **438**, L25
- Chinchilla P., et al., 2020, *A&A*, **633**, A152
- Cruz K. L., Kirkpatrick J. D., Burgasser A. J., 2009, *AJ*, **137**, 3345
- Cutri R. M., et al. 2014, *VizieR Online Data Catalog*, **2328**, 0
- D’Odorico S., et al., 2006, in *Society of Photo-Optical Instrumentation Engineers (SPIE) Conference Series*. , [doi:10.1117/12.672969](#)
- De Gennaro S., von Hippel T., Jefferys W. H., Stein N., van Dyk D., Jeffery E., 2009, *ApJ*, **696**, 12
- Delorme P., Collier Cameron A., Hebb L., Rostron J., Lister T. A., Norton A. J., Pollacco D., West R. G., 2011, *MNRAS*, **413**, 2218
- Desrochers M.-E., Artigau É., Gagné J., Doyon R., Malo L., Faherty J. K., Lafrenière D., 2018, *ApJ*, **852**, 55
- Duchêne G., Kraus A., 2013, *ARA&A*, **51**, 269
- Duchêne G., Bouvier J., Moraux E., Bouy H., Konopacky Q., Ghez A. M., 2013, *A&A*, **555**, A137
- Dupuy T. J., Liu M. C., 2012, *ApJS*, **201**, 19
- Dupuy T. J., Liu M. C., 2017, *ApJS*, **231**, 15
- Filippazzo J. C., Rice E. L., Faherty J., Cruz K. L., Van Gordon M. M.,Looper D. L., 2015, *ApJ*, **810**, 158
- Fossati L., Bagnulo S., Landstreet J., Wade G., Kochukhov O., Monier R., Weiss W., Gebran M., 2008, *A&A*, **483**, 891
- Fukugita M., Ichikawa T., Gunn J. E., Doi M., Shimasaku K., Schneider D. P., 1996, *AJ*, **111**, 1748
- Gaia Collaboration et al., 2018a, *A&A*, **616**, A1
- Gaia Collaboration et al., 2018b, *A&A*, **616**, A10
- Gizis J., Reid I. N., 1995, *AJ*, **110**, 1248
- Goldoni P., Royer F., François P., Horrobin M., Blanc G., Vernet J., Modigliani A., Larsen J., 2006, in *Society of Photo-Optical Instrumentation Engineers (SPIE) Conference Series*. , [doi:10.1117/12.669986](#)

- Golimowski D. A., et al., 2004, *AJ*, **127**, 3516
- González-García B. M., Zapatero Osorio M. R., Béjar V. J. S., Bihain G., Barrado y Navascués D., Caballero J. A., Morales-Calderón M., 2006, *A&A*, **460**, 799
- Gossage S., Conroy C., Dotter A., Choi J., Rosenfield P., Cargile P., Dolphin A., 2018, *ApJ*, **863**, 67
- Hambly N. C., Steele I. A., Hawkins M. R. S., Jameson R. F., 1995, *MNRAS*, **273**, 505
- Hambly N. C., et al., 2008, *MNRAS*, **384**, 637
- Hewett P. C., Warren S. J., Leggett S. K., Hodgkin S. T., 2006, *MNRAS*, **367**, 454
- Hodgkin S. T., Irwin M. J., Hewett P. C., Warren S. J., 2009, *MNRAS*, **394**, 675
- Hogan E., Jameson R. F., Casewell S. L., Osbourne S. L., Hambly N. C., 2008, *MNRAS*, **388**, 495
- Joergens V., 2006, *A&A*, **446**, 1165
- Joergens V., 2008, *A&A*, **492**, 545
- Joergens V., Müller A., 2007, *ApJL*, **666**, L113
- Kendall T. R., Delfosse X., Martín E. L., Forveille T., 2004, *A&A*, **416**, L17
- Khalaj P., Baumgardt H., 2013, *MNRAS*, **434**, 3236
- Kirkpatrick J. D., et al., 2000, *AJ*, **120**, 447
- Kirkpatrick J. D., et al., 2008, *ApJ*, **689**, 1295
- Kirkpatrick J. D., et al., 2010, *ApJS*, **190**, 100
- Konopacky Q. M., Ghez A. M., Rice E. L., Duchêne G., 2007, *ApJ*, **663**, 394
- Kraus A. L., Hillenbrand L. A., 2007, *AJ*, **134**, 2340
- Kraus A. L., Hillenbrand L. A., 2012, *ApJ*, **757**, 141
- Kraus A. L., White R. J., Hillenbrand L. A., 2005, *ApJ*, **633**, 452
- Kraus A. L., White R. J., Hillenbrand L. A., 2006, *ApJ*, **649**, 306
- Larkin J., et al., 2006, in Society of Photo-Optical Instrumentation Engineers (SPIE) Conference Series. p. 62691A, doi:10.1117/12.672061
- Lawrence A., Warren S. J., Almaini O., Edge A. C., Hambly N. C., 17 co-authors 2007, *MNRAS*, **379**, 1599
- Lawrence A., et al., 2013, VizieR Online Data Catalog, p. II/319
- Lebreton Y., Fernandes J., Lejeune T., 2001, *A&A*, **374**, 540
- Lindgren L., et al., 2018, *A&A*, **616**, A2
- Liu Y.-J., et al., 2008, *ApJ*, **672**, 553
- Lodieu N., Boudreault S., Béjar V. J. S., 2014, *MNRAS*, **445**, 3908
- Lodieu N., Zapatero Osorio M. R., Béjar V. J. S., Peña Ramírez K., 2018a, *MNRAS*, **473**, 2020
- Lodieu N., Rebolo R., Pérez-Garrido A., 2018b, *A&A*, **615**, L12
- Lodieu N., Pérez-Garrido A., Smart R. L., Silvotti R., 2019, *A&A*, **628**, A66
- Maeder A., Mermilliod J. C., 1981, *A&A*, **93**, 136
- Manjavacas E., Lodieu N., Béjar V. J. S., Zapatero-Osorio M. R., Boudreault S., Bonnefoy M., 2020, *MNRAS*, **491**, 5925
- Martín E. L., Brandner W., Bouvier J., Luhman K. L., Stauffer J., Basri G., Zapatero Osorio M. R., Barrado y Navascués D., 2000, *ApJ*, **543**, 299
- Martín E. L., Barrado y Navascués D., Baraffe I., Bouy H., Dahm S., 2003, *ApJ*, **594**, 525
- Martín E. L., Lodieu N., Pavlenko Y., Béjar V. J. S., 2018, *ApJ*, **856**, 40
- Mazzei P., Pigatto L., 1988, *A&A*, **193**, 148
- Mermilliod J. C., 1981, *A&A*, **97**, 235
- Modigliani A., et al., 2010, in Society of Photo-Optical Instrumentation Engineers (SPIE) Conference Series. , doi:10.1117/12.857211
- Mohanty S., Jayawardhana R., Huélamo N., Mamajek E., 2007, *ApJ*, **657**, 1064
- Naud M.-E., Artigau É., Doyon R., Malo L., Gagné J., Lafrenière D., Wolf C., Magnier E. A., 2017, *AJ*, **154**, 129
- Ochsenbein F., Bauer P., Marcout J., 2000, *A&AS*, **143**, 23
- Oke J. B., 1990, *AJ*, **99**, 1621
- Pecaut M. J., Mamajek E. E., 2013, *ApJS*, **208**, 9
- Pinfield D. J., Hodgkin S. T., Jameson R. F., Cossburn M. R., von Hippel T., 1997, *MNRAS*, **287**, 180
- Ruiz M. T., Leggett S. K., Allard F., 1997, *ApJL*, **491**, L107
- Scardia M., et al., 2007, *MNRAS*, **374**, 965
- Schmidt S. J., West A. A., Hawley S. L., Pineda J. S., 2010, *AJ*, **139**, 1808
- Service M., Lu J. R., Campbell R., Sitarski B. N., Ghez A. M., Anderson J., 2016, *PASP*, **128**, 095004
- Stassun K. G., Mathieu R. D., Valenti J. A., 2006, *Nature*, **440**, 311
- Stauffer J. R., Schultz G., Kirkpatrick J. D., 1998, *ApJL*, **499**, 199
- Tecza M., Thatte N., Clarke F., Freeman D., 2009, *Astrophysics and Space Science Proceedings*, **9**, 267
- Thatte N., et al., 2010, in Ground-based and Airborne Instrumentation for Astronomy III. p. 77352I, doi:10.1117/12.857445
- Theodossiou E., Danezis E., 1991, *Astrophys. Space. Sci.*, **183**, 91
- Todorov K., Luhman K. L., McLeod K. K., 2010, *ApJL*, **714**, L84
- Todorov K. O., Luhman K. L., Konopacky Q. M., McLeod K. K., Apai D., Ghez A. M., Pascucci I., Robberto M., 2014, *ApJ*, **788**, 40
- Tody D., 1986, in Crawford D. L., ed., Society of Photo-Optical Instrumentation Engineers (SPIE) Conference Series Vol. 627, Society of Photo-Optical Instrumentation Engineers (SPIE) Conference Series. p. 733
- Tody D., 1993, in Hanisch R. J., Brissenden R. J. V., Barnes J., eds, Astronomical Society of the Pacific Conference Series Vol. 52, Astronomical Data Analysis Software and Systems II. p. 173
- Tokunaga A. T., Simons D. A., Vacca W. D., 2002, *PASP*, **114**, 180
- Vernet J., et al., 2011, *A&A*, **536**, A105
- Vrba F. J., et al., 2004, *AJ*, **127**, 2948
- Wang W., Boudreault S., Goldman B., Henning T., Caballero J. A., Bailer-Jones C. A. L., 2011, *A&A*, **531**, A164
- Wang P. F., et al., 2014, *ApJ*, **784**, 57
- Watson A. M., et al., 2016, in Ground-based and Airborne Instrumentation for Astronomy VI. p. 99080P (arXiv:1605.09660), doi:10.1117/12.2233069
- Wizinowich P. L., et al., 2006, *PASP*, **118**, 297
- Wright E. L., Eisenhardt P. R. M., Mainzer A. K., Ressler M. E., Cutri R. M., Jarrett T., Kirkpatrick J. D., 31 co-authors 2010, *AJ*, **140**, 1868
- Zapatero Osorio M. R., Lane B. F., Pavlenko Y., Martín E. L., Britton M., Kulkarni S. R., 2004, *ApJ*, **615**, 958
- del Burgo C., Allende Prieto C., 2018, *MNRAS*, **479**, 1953
- van Dam M. A., et al., 2006, *PASP*, **118**, 310

This paper has been typeset from a  $\text{\TeX}/\text{\LaTeX}$  file prepared by the author.